NASA TECHNICAL NOTE

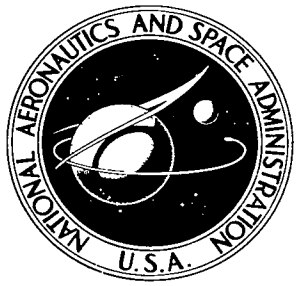










# CONVECTIVE HEAT-TRANSFER RATES ON A BLUNTED 110° CONE WITH HEMISPHERICAL AFTERBODY AT HYPERSONIC SPEEDS

*by David A. Stewart*

*Ames Research Center*
*Moffett Field, Calif. 94035*

NATIONAL AERONAUTICS AND SPACE ADMINISTRATION • WASHINGTON, D. C. • JULY 1971

| 1. Report No. | 2. Government Accession No. | 3. Recipient's Catalog No. |
|---|---|---|
| NASA TN D-6433 | | |

| 4. Title and Subtitle | 5. Report Date |
|---|---|
| CONVECTIVE HEAT-TRANSFER RATES ON A BLUNTED 110° CONE WITH HEMISPHERICAL AFTERBODY AT HYPERSONIC SPEEDS | July 1971 |
| | 6. Performing Organization Code |

| 7. Author(s) | 8. Performing Organization Report No. |
|---|---|
| David A. Stewart | A-3970 |
| | 10. Work Unit No. |
| 9. Performing Organization Name and Address | 129-01-20-01-00-21 |
| NASA—Ames Research Center<br>Moffett Field, Calif. 94035 | 11. Contract or Grant No. |
| | 13. Type of Report and Period Covered |
| 12. Sponsoring Agency Name and Address | Technical Note |
| National Aeronautics and Space Administration<br>Washington, D. C. 20546 | 14. Sponsoring Agency Code |

15. Supplementary Notes

16. Abstract

Heat-transfer rates were measured on a one-sixth scale model of the Ames Planetary Atmosphere Experimental Test (PAET) configuration which consists of a blunted 55° half-angle cone with spherical segment nose cap and hemispherical afterbody. The investigation was conducted in the Ames 42-Inch Shock Tunnel and the Ames Hypersonic Free-Flight Facility at Mach numbers of 7 and 15, Reynolds numbers of 300,000, 100,000, and 15,500, and angles of attack from 0° to 25°. From existing theories of inviscid flow, which include the bow-wave shape and the large pressure gradients near the sharp corner, the surface heating-rate distribution is predicted at $\alpha = 0°$. High heat-transfer rates occurred near the sharp corner of the PAET model at all angles of attack because of local pressure gradients. In general, the pattern of forebody heating-rate distribution with increased angle of attack was higher to windward and lower to leeward. The heating rates on the hemispherical afterbody did not exceed 20 percent of the reference stagnation value. An order-of-magnitude increase in Reynolds number influenced heating only near the corner of the forebody, where local values decreased from 60 to 30 percent as the angle of attack was increased from $\alpha = 0°$ to 10°.

Bow-wave profiles were taken during the heat-transfer tests at angles of attack from 0° to 25°. An observed inflection in the bow-wave at $\alpha = 0°$ and $\alpha = 10°$ is attributed to three-dimensional effects in the inviscid flow; in the present investigation, this inflection had no discernible effect on surface heating.

| 17. Key Words (Suggested by Author(s)) | 18. Distribution Statement |
|---|---|
| PAET<br>Blunt-body heat transfer | Unclassified – Unlimited |

| 19. Security Classif. (of this report) | 20. Security Classif. (of this page) | 21. No. of Pages | 22. Price* |
|---|---|---|---|
| Unclassified | Unclassified | 20 | $3.00 |

*For sale by the National Technical Information Service, Springfield, Virginia 22151

## SYMBOLS

| | |
|---|---|
| A,B,C,D | constants |
| $C_p$ | specific heat of model material |
| g | normalized total enthalpy, $H/H_o$ |
| H | total enthalpy |
| M | Mach number |
| p | pressure |
| $\dot{q}$ | heating rate |
| R | radius |
| $Re_D$ | Reynolds number (free-stream Reynolds number based on diameter) |
| $\bar{r}$ | radius of cross section of body of revolution |
| S | surface distance from center of nose |
| S* | surface distance from center of nose to sonic point |
| T | absolute temperature |
| u | velocity |
| x,y | cylindrical coordinates |
| $\alpha$ | angle of attack |
| $\delta$ | cone half-angle |
| $\rho$ | density |
| $\tau$ | model skin thickness |

### Subscripts

| | |
|---|---|
| a | afterbody |
| b | base of body |

| | |
|---|---|
| c | corner |
| e | outer edge of the boundary layer |
| n | nose |
| o | model stagnation point |
| w | model wall condition |
| $\infty$ | free stream |
| * | sonic point |

# CONVECTIVE HEAT–TRANSFER RATES ON A BLUNTED 110° CONE WITH HEMISPHERICAL AFTERBODY AT HYPERSONIC SPEEDS

David A. Stewart

Ames Research Center

## SUMMARY

Heat-transfer rates were measured on a one-sixth scale model of the Ames Planetary Atmosphere Experimental Test (PAET) configuration which consists of a blunted 55° half-angle cone with spherical segment nose cap and hemispherical afterbody. The investigation was conducted in the Ames 42-Inch Shock Tunnel and the Ames Hypersonic Free-Flight Facility at Mach numbers of 7 and 15, Reynolds numbers of 300,000, 100,000, and 15,500, and angles of attack from 0° to 25°. From existing theories of inviscid flow, which include the bow-wave shape and the large pressure gradients near the sharp corner, the surface heating-rate distribution is predicted at $\alpha = 0°$. High heat-transfer rates occurred near the sharp corner of the PAET model at all angles of attack because of local pressure gradients. In general, the pattern of forebody heating-rate distribution with increased angle of attack was higher to windward and lower to leeward. The heating rates on the hemispherical afterbody did not exceed 20 percent of the reference stagnation value. An order-of-magnitude increase in Reynolds number influenced heating only near the corner of the forebody, where local values decreased from 60 to 30 percent as the angle of attack was increased from $\alpha = 0°$ to 10°.

Bow-wave profiles were taken during the heat-transfer tests at angles of attack from 0° to 25°. An observed inflection in the bow-wave at $\alpha = 0°$ and $\alpha = 10°$ is attributed to three-dimensional effects in the inviscid flow; in the present investigation, this inflection had no discernible effect on surface heating.

## INTRODUCTION

The primary objective of the Ames Planetary Atmosphere Experiments Test Project (PAET) is to demonstrate, in the earth's atmosphere, the usefulness of various entry vehicle experiments in determining the structure and composition of an unknown planetary atmosphere. The PAET configuration (a 55° half-angle blunted cone with a hemispherical afterbody) and on-board instrumentation concepts were derived from a number of theoretical and experimental investigations (refs. 1 through 10). Studies on large-angle conical bodies of this type show that the inviscid flow over the forebody surface may well be subsonic (refs. 11, 12). Consequently, very substantial convective heating rates may occur in the region of the sharp corner because of the large pressure gradients in this area (refs. 13, 14).

During entry into the earth's atmosphere, maximum heating rates to the PAET vehicle are expected to occur at an altitude at 52.6 km, a flight velocity of 6.69 km/s, $M_\infty = 15$, and

a $Re_D$ = 300,000 (based on vehicle diameter of 0.9 m). To ensure the adequacy of the PAET afterbody TPS system (ref. 15), a heat-transfer investigation was conducted in two different facilities: the Ames 42-Inch Shock Tunnel and in the Ames Hypersonic Free-Flight Aerodynamic Facility. The investigation was performed in air at a Mach number of 7, Reynolds numbers of 100,000, and 300,000 (based on model diameter) and total enthalpy of 1750 J/g in the Ames Hypersonic Free-Flight Facility and at a Mach number of 15, Reynolds number of 15,500 (based on model diameter), and total enthalpy of 9,300 J/g in the Ames 42-Inch Shock Tunnel. The results of this investigation were used as an input in an analytical definition of the structural temperature at various positions on the PAET afterbody (ref. 16).

## FACILITIES

The 42-inch shock tunnel (refs. 17-18) uses combustion-heated driver gas to produce a reflected shock, tailored-interface reservoir of heated air at the end of a shock tube 12.2 m long and 15.75 cm in diameter. For these tests the reservoir pressure and enthalpy were 286 atm and 9300 J/g, respectively. The reservoir gas was expanded through a 20° conical nozzle to generate a flow in the test region at Mach number 15 and a velocity of 4160 m/s. The corresponding Reynolds number, based on body diameter, was 15,500. The flow duration for each test was 20 ms.

The Hypersonic Free-Flight Aerodynamic Facility (H.F.F., ref. 19) uses cold helium driver gas to produce a reflected-shock, tailored-interface reservoir of test gas at the end of a shock tube 25.9 m long and 30.5 cm in diameter. Reservoir pressures were 10.88 and 32.65 atm, both at an enthalpy of 1750 J/g. The reservoir gas (air) was expanded through a contoured nozzle to a Mach number of 7 at a velocity of 1873 m/s, in the test section. The corresponding Reynolds numbers for the two test conditions were 100,000 and 300,000 based on body diameter. The results were obtained from each of these tests during the first 10 ms of tunnel flow.

## MODEL

The one-sixth scale model (fig. 1) is a 55° half-angle cone with a base radius of 7.56 cm, spherical nose cap, and hemispherical afterbody. A sharp corner exists at the juncture of the nose cone and the spherical afterbody. The nose-to-body radius ratio is unity. The model was designed to minimize heat-conduction errors in the region of the corner. The 0.043-cm thick copper forebody and afterbody were joined with an epoxy cement and secured to three longitudinal braces. Application of epoxy within 1.25 cm of the thermocouple arrays was carefully avoided. As shown in figure 1, the main array extended around the model in the pitch plane and consisted of 16 thermocouples. Two additional thermocouples were located on the afterbody surface near the sharp corner, at 90° from the main thermocouple array. Each thermocouple junction was made by drilling two small holes 0.051 cm apart in the model wall and soldering a pair of number 40 gage chromel-constantan wires in these holes. The response time of the junctions is estimated to be less than 1 ms. This model was used for the tests in both facilities.

## INSTRUMENTATION AND DATA REDUCTION

Flow-visualization (self-luminous) pictures and shadowgraphs were taken during the tests to define the contour of the bow wave. The self-luminous pictures were taken during the tests in the 42-inch shock tunnel, using a high-speed shutter (1/1000 s) to control the exposure of EKTA–S film. The solenoid-operated shutter was pulsed so that it opened at approximately 5 ms after the flow started.

Shadowgraphs taken during tests in the H.F.F. facility were obtained with a single-path system having a spark-gap with a 0.10-cm diameter aperture at the source.

The convective heat-transfer data taken in the 42-inch shock tunnel were obtained by measuring the rate of increase of model wall temperature during the test time of approximately 20 ms. Thermocouple emf outputs were amplified and recorded on a high-speed oscillograph. The temperature-time traces were curve-fitted with a seventh-order polynomial to obtain local slopes. Heat-transfer rates at a given time were determined from the equation

$$\dot{q} = \rho C_p \tau (dT/dt) \tag{1}$$

with an estimated maximum error of ±10 percent. Further details regarding data reduction and testing techniques are given in reference 18.

The convective heat-transfer rates were obtained in a similar manner for the tests in the H.F.F. facility. The thermocouple outputs were amplified and recorded on oscilloscopes. The temperature-time data were reduced by a straight line curve fit to the oscilloscope record. Average heat-transfer rates for a 10-ms time period were determined using equation (1) above. The estimated maximum heat-transfer error-band for these data was ±20 percent over the model afterbody and ±15 percent over the model forebody.

## RESULTS AND DISCUSSION

### Body Flow Field

As a requirement in predicting and interpreting the heat-transfer data for the PAET configuration, the flow field is discussed in some detail, and illustrated by shadowgraphs and flow visualization pictures taken during the investigation.

*Bow wave*– At zero angle of attack an inflection (reverse curvature) in the bow wave occurred in the region of the corner (fig. 2). In the shadowgraphs taken during the tests in the H.F.F. facility, this inflection is more pronounced over the upper portion of the body, possibly because of a small model misalinement. At $\alpha = 10°$, the inflection in the bow wave is present only in the flow field over the upper portion of the body, while at $\alpha > 10°$, it disappears and the entire bow wave becomes approximately spherical in shape. Reynolds number and Mach number had little effect on the observed inflection.

This type of nonuniformity in the bow shock wave has been reported in references 20 to 22. In particular, Cleary (ref. 21) shows it to be characteristic of three-dimensional expanding flow downstream of a blunt nose, wherein to satisfy the flow continuity the entropy layer and shock layer become thinner and the maximum pressure streamline closely approaches the surface. The effect is accentuated by increasing the inclination of the windward surface and persists into the regime of locally subsonic flow (ref. 22). The same three-dimensional behavior is thought to account for the observed bow-wave inflection in the present tests.

*Inviscid flow*– The inviscid flow properties required to predict the surface heating rates for configurations of this general shape are usually approximated using Newtonian theory. In the present case, the cone angle of 55° is within a rather unique and narrow range wherein the flow within the shock layer can be a mixture of subsonic and supersonic flow and Newtonian theory is not valid. Therefore, in obtaining the flow properties, it was assumed that the bow-wave shape was a hyperbola and the numerical solution of Garabedian and Lieberstein (ref. 23) was used. This numerical solution is for a body of infinite length, and the sonic line and surface pressure distribution will depart from the prediction as the sharp corner of the truncated body is approached. The portion of the flow over the truncated cone cannot be predicted exactly; however, an approximate method, suggested by Kaattari (ref. 24), can be used to estimate the inviscid flow properties near the corner.

At zero angle of attack the bow-wave coordinates from the shadowgraph (fig. 2) for $M_\infty = 7.0$ and $\gamma = 1.4$ are compared in figure 3 with the results of a numerical solution (ref. 23) for $M_\infty = 5.8$ and $\gamma = 1.4$.[1] The predicted bow-wave geometry agrees well with the experimental data except in the inflection region. The resulting forebody contour closely matches the physical shape except for a small difference near the sharp corner. Included in figure 3 is the sonic line predicted from the numerical solution; it originates near the inflection of the experimental bow wave and asymptotically approaches the infinite-body surface. Truncating the conical body, as mentioned earlier, must modify the infinite-body inviscid flow by forcing the sonic line to terminate at the sharp corner. The details of this local singular behavior cannot be predicted by the numerical analysis; however, it follows that a substantial pressure gradient must exist near the corner to force the surface pressure to the sonic value.

The pressure variation along the forward surface of the model is predicted by joining results from the numerical solution to a Prandtl-Meyer expansion at the corner using a connecting link, after the manner described in reference 24. The pressure distribution near the corner can be approximated by the first four terms of the following Taylor series:

$$S/S^* = A - B(p/p_O) + C(p/p_O)^2 - D(p/p_O)^3 \qquad (2)$$

The emphasis on obtaining a realistic prediction in the corner region is justified by prior knowledge that local subsonic expansions of this type can increase local heating rates, and that such increases were in fact observed in the present experiments. The results are shown in figure 4, where the composite prediction is compared to the simple Newtonian pressure distribution. The afterbody flow behind the corner is treated, in steps, as a local two-dimensional expansion.

---

[1] The available solution at $M_\infty = 5.8$ is sufficiently close to the test Mach number that a direct comparison can be made for this large-angle blunted cone. The well-known invariance of blunt-body shock layers at $M_\infty > 3$ is demonstrated again in reference 25 for a shape similar to that used here.

## Heat-Transfer Rates

*Zero angle of attack*– Once the inviscid flow over the PAET configuration has been determined, one may use the resulting pressure distribution in conjunction with the theory of Kemp, Rose, and Detra (ref. 26) as modified by Marvin (ref. 13):

$$\dot{q}_w/\dot{q}_{w_o} = \left\{(p/p_o)(u_e/u_\infty)\bar{r}/2\left[\int_o^s (p/p_o)(u_e/u_\infty)(\bar{r})^2\, ds\right]^{1/2}[(l/u_\infty)(du_e/ds)_o]^{1/2}\right\}[g'(o)/g'_o(o)] \tag{3}$$

where $g'(o)/g'_o(o)$ relates implicitly the surface pressure-gradient effect on the heat-transfer rate distribution. Two solutions are calculated using equation (3) with the pressure distribution predicted by the composite numerical solution. First, for $g'(o)/g'_o(o) = 1.0$, the effect of pressure gradients on the boundary-layer flow over the surface is neglected. Second, $g'(o)/g'_o(o)$ is calculated from a correlation equation based on locally similar boundary-layer solutions.

The theoretical heating rate distributions for $\alpha = 0°$ are compared with the experiment in figure 5. Local heating rates are normalized by the stagnation point heating rate at $\alpha = 0°$ and plotted against the ratio of arc length to nose radius. The data from both shock-tunnel facilities agree well, except near the sharp corner at $S/R_n = 1.112$, where the difference in heating rate was 50 percent. Also, at the sharp corner the heating rate was observed to be from 30 to 60 percent above the value at $S/R_n = 0.87$. On the afterbody the heating rates near the corner are approximately 10 percent of the stagnation value and fall substantially below this value downstream.

The theoretical predictions for the blunt forebody agree well with the experimental data at both Mach numbers and the high heating rate near the sharp corner is reasonably predicted by equation (3) using $g'(o)/g'_o(o)$ from a correlation equation for locally similar boundary-layer solutions. (Note that Lees' theory for heat-transfer distribution (ref. 27), usually used for this type of body, would predict essentially the same result as equation (3) with $g'(o)/g'_o(o) = 1.0$.) Equation (3) underpredicts the heating rates uniformly over the afterbody by 40 percent. This result implies two things about the flow: The local pressures are higher than predicted, and the flow behind the corner may not be completely separated from the surface. The relative importance of these two effects can only be resolved by further experiment.

*Angle of attack to 25°*– Figure 6 shows heat-transfer data on the PAET configuration for angles of attack of 10°, 15°, 20°, and 25°. Note that $S/R_n = 0$ is located at the geometric center of the spherical nose cap, while the windward and leeward direction of flow along the model surface are referenced to the Newtonian stagnation-point location. Curves have been faired through the data to aid in the interpretation.

The level of heat-transfer rates on the windward side of the forebody tends to increase with increasing angle of attack, while at the sharp corner the local maximum persists. The consistent high heating rate at the sharp corner is attributed to the high local pressure gradient existing in the subsonic inviscid flow. An anomalous behavior occurs at $\alpha = 20°$, where the heating rates in the stagnation region of the model at $S/R_n < 0.8$ are lower than for either $\alpha = 15°$ or 25°. This is intuitively thought to result from a decrease in local velocity gradients as the flow adjusts to the presence of the adjacent conical surface. The consistency of the data over the Mach and Reynolds number range investigated indicates the phenomenon to be real.

On the windward side of the afterbody heating rates near the sharp corner ($S/R_n < 1.3$) increased from approximately $\dot{q}_w/\dot{q}_{w_o} = 0.08$ to 0.16 with an increase in angle of attack from $\alpha = 10°$ to $\alpha = 25°$. At surface distances $S/R_n \geq 1.80$, rates were less than $\dot{q}_w/\dot{q}_{w_o} = 0.04$ for all angles of attack. Here again there are definite indications of attached flow for a short distance behind the corner, followed by separation and heating rates invariant with angle of attack. Because of uncertainty in the higher Reynolds number data, it is not possible to isolate Reynolds number effects on the afterbody heating.

The heating rates on the leeward side of the conical forebody decrease from $\dot{q}_w/\dot{q}_{w_o} = 0.58$ to $\dot{q}_w/\dot{q}_{w_o} = 0.28$ as angle of attack increases from $\alpha = 10°$ to 25°, while the "hot corner" disappears to $\alpha > 10°$. This behavior, of course, is indicative of supersonic inviscid flow over this region. On the leeward side of the afterbody, heating rates remained roughly constant at $\dot{q}_w/\dot{q}_{w_o} = 0.05$ for all angles of attack between $\alpha = 10°$ and 25°. No attempt was made to predict the heating rate at angle of attack because of the complexity of the inviscid flow.

## CONCLUSIONS

Convective heating-rate distributions were investigated on the Planetary Atmosphere Experimental Test configuration in the Ames Hypersonic Free-Flight Facility at Mach number 7 for Reynolds numbers of 300,000 and 100,000 and in the Ames 42-Inch Shock Tunnel at Mach number 15 with Reynolds number 15,500 using air as the test medium. The shock layer over the blunted, 55° conical forebody is composed of partly subsonic, partly supersonic flow. At zero angle of attack the sonic line originates at the bow wave in the vicinity of the sphere-cone intersection, while at $\alpha > 0°$ the windward flow becomes progressively more subsonic and the leeward supersonic. An inflection in the bow wave that occurs at $\alpha$ up to 10° is attributed to three-dimensional effects in the inviscid flow and causes no discernible disturbance in surface heating.

The following conclusions result from these tests:

1. A region of high heating exists on the forebody near the sharp corner at $\alpha = 0°$ and windward at angles of attack up to 25° because of a substantial local pressure gradient (flow acceleration) in the subsonic flow.

2. Heating-rate distributions can be predicted over the forebody at $\alpha = 0°$, from existing theories of inviscid flow, if the bow-wave shape is known and the influence of large pressure gradients near the sharp corner is included. Conversely, afterbody heating rates cannot be predicted within a factor of two using a two-dimensional expansion to calculate inviscid flow throughout this region.

3. The pattern of forebody heating with increasing angle of attack, higher to windward and lower to leeward, is interrupted at $\alpha = 20°$ by an anomalous decrease of 30 percent in the stagnation region, indicating a reduction in local velocity gradients as the flow adjusts to the presence of the conical surface.

4. Heating rates on the spherical afterbody did not exceed 20 percent of the reference stagnation value. Comparison with theory indicates a region of flow attachment behind the body corner at $\alpha = 0°$ and on the windward side at angles of attack up to 25°.

5. An order-of-magnitude increase in Reynolds number influenced heating only near the corner on the forebody, where local values were decreased from 60 to 30 percent at $\alpha = 0°$ and 10°

Ames Research Center
National Aeronautics and Space Administration
Moffett Field, Calif., 94035, May 10, 1971

## REFERENCES


1. Seiff, Alvin: Some Possibilities for Determining the Characteristics of the Atmosphere of Mars and Venus From Gas-Dynamic Behavior of a Probe Vehicle. NASA TN D–1770, 1963.

2. Seiff, Alvin; and Reese, David E., Jr.: Defining Mars' Atmosphere – A Goal for the Early Missions. Astronaut. Aeron., vol. 3, no. 2, Feb. 1965, pp. 16-21.

3. Seiff, Alvin; and Reese, David E., Jr.: Use of Entry Vehicle Responses to Define the Properties of the Mars Atmosphere. Proc. Am. Astronautical Soc. Symp. on the Unmanned Exploration of the Solar System, Denver, Colorado, Feb. 8-10, 1965, Preprint 65–24.

4. Peterson, Victor L.: A Technique for Determining Planetary Atmosphere Structures From Measured Accelerations of an Entry Vehicle. NASA TN D–2669, 1965.

5. Peterson, Victor L.: Analysis of the Errors Associated With the Determination of Planetary Atmosphere Structure From Measured Accelerations of an Entry Vehicle. NASA TR R–225, 1965.

6. Reese, David E., Jr.; and Georgiev, Steven: Design Problems and Experiments for Mars Atmosphere Probes. AIAA/AAS Stepping Stones to Mars Meeting, Baltimore, Maryland, March 1966. Technical Papers, AIAA, N. Y., 1966, pp. 542-552.

7. Whiting, Ellis E.: Determination of Mars Atmospheric Composition by Shock-Layer Radiometry During a Probe Experiment. AIAA Preprint 67–293, 1967.

8. Georgiev, Steven: A Feasibility Study of an Experiment for Determining the Properties of the Mars Atmosphere. Vol. I, Summary, NASA CR–530, 1967. Vol. II, Probe System Selection and Design, NASA CR–73004, 1966. Vol. III, Subsystem and Technical Analysis, NASA CR–73005, 1966. Vol. IV, Sterilization Analysis, NASA CR–73006, 1966. Vol. V, Probe Development Plan, NASA CR–73007, 1966. Vol. VI, Venus Probe Analysis and Design, NASA CR–73008, 1966.

9. Sommer, Simon C.; Boissevain, Alfred G.; Yee, Layton; and Hedlund, Roger: The Structure of an Atmosphere From On-Board Measurements of Pressure, Temperature, and Acceleration. NASA TN D–3933, 1967.

10. Sommer, Simon C.; and Yee, Layton: An Experiment to Determine the Structure of a Planetary Atmosphere. AIAA Preprint 68–1054, J. Spacecraft and Rockets, vol. 6, June 1969, pp. 704-710.

11. Stewart, David A.; and Inouye, Mamoru: Shock Shapes and Pressure Distributions for Large-Angle Pointed Cones in Helium at Mach Numbers of 8 and 20. NASA TN D–5343, 1969.

12. Campbell, James F.; and Tudor, Dorothy H.: Pressure Distributions on 140°, 160°, and 180°, Cones at Mach Numbers From 2.30 to 4.63 and Angles of Attack From 0° to 20°. NASA TN D–5204, 1969.

13. Marvin, Joseph G.; and Sinclair, A. Richard: Convective Heating in Regions of Large Favorable Pressure Gradient. AIAA J., vol. 5, no. 11, Nov. 1967, pp. 1940-1948.

14. Stewart, David A.; and Marvin, Joseph G.: Convective Heat-Transfer Rates on Large-Angle Conical Bodies at Hypersonic Speeds. NASA TN D–5526, 1969.

15. Carlson, David L.: Heat Shields for Planetary Atmospheric Experiments Test (PAET) Probe. Final Report. Vol. 1, Martin Marietta Corp., Denver, Colorado, MCR–70–170 (Contract NAS 2–5538), May 20, 1970.

16. Carlson, David L.: Thermal Analysis of the PAET Afterbody Heat Shield System. MCR–70–464, Martin Marietta Corp., Denver, Colorado (Contract NAS 2–6274), Dec. 1970.

17. Loubsky, William J.; Hiers, Robert S.; and Stewart, David A.: Performance of a Combustion-Drive Shock Tunnel With Application to the Tailored-Interface Operating Conditions. Vol. 2 of The Performance of High Temperature Systems, Proc. Third Conf., Gilbert S. Bahn, ed., Gordon and Breach, N. Y., pp. 547-559.

18. Hiers, Robert S., Jr.; and Reller, John O., Jr.: Analysis of Nonequilibrium Air Streams in the Ames 1-Foot Shock Tunnel. NASA TN D–4985, 1969.

19. DeRose, Charles E.: Trim Attitude Lift and Drag of the Apollo Command Module With Offset Center-of-Gravity Positions at Mach Numbers to 29. NASA TN D–5276, 1969.

20. Seiff, Alvin; Sommer, Simon C.; and Canning, Thomas N.: Some Experiments at High Supersonic Speeds on the Aerodynamic and Boundary-Layer Transition Characteristics of High-Drag Bodies of Revolution. NACA RM A56105, 1957.

21. Cleary, Joseph W.: An Experimental and Theoretical Investigation of the Pressure Distribution and Flow Fields of Blunted Cones at Hypersonic Mach Numbers. NASA TN D–2969, 1965.

22. Cleary, Joseph W.; and Duller, Charles E.: Effects of Angle of Attack and Bluntness on the Hypersonic Flow Over a 15° Semiapex Cone in Helium. NASA TN D–5903, 1970.

23. Garabedian, P. R.; and Lieberstein, H. M.: On the Numerical Calculation of Detached Bow Shock Waves in Hypersonic Flow. J. Aero. Sci., vol. 25, no. 2, Feb. 1958, pp. 109-118.

24. Kaattari, George E.: A Method for Predicting Shock Shapes and Pressure Distribution for a Wide Variety of Blunt Bodies of Zero Angle of Attack. NASA TN D–4539, 1968.

25. Stallings, Robert L., Jr.; and Tudor, Dorothy H.: Experimental Pressure Distributions on a 120° Cone at Mach Numbers From 2.96 to 4.63 and Angle of Attack 0° to 20°. NASA TN D–5054, 1969.

26. Kemp, Nelson H.; Rose, Peter H.; and Detra, Ralph W.: Laminar Heat Transfer Around Blunt Bodies in Dissociated Air. Res. Rep. 15, AVCO Res. Lab., Everett, Mass., 1958. (Also J. Aerospace Sci., vol. 26, no. 7, July 1959, pp. 421-430.)

27. Lees, Lester: Laminar Heat Transfer Over Blunt-Nosed Bodies at Hypersonic Flight Speed. Jet Propulsion, vol. 26, no. 4, Apr. 1956, pp. 259-269, 274.

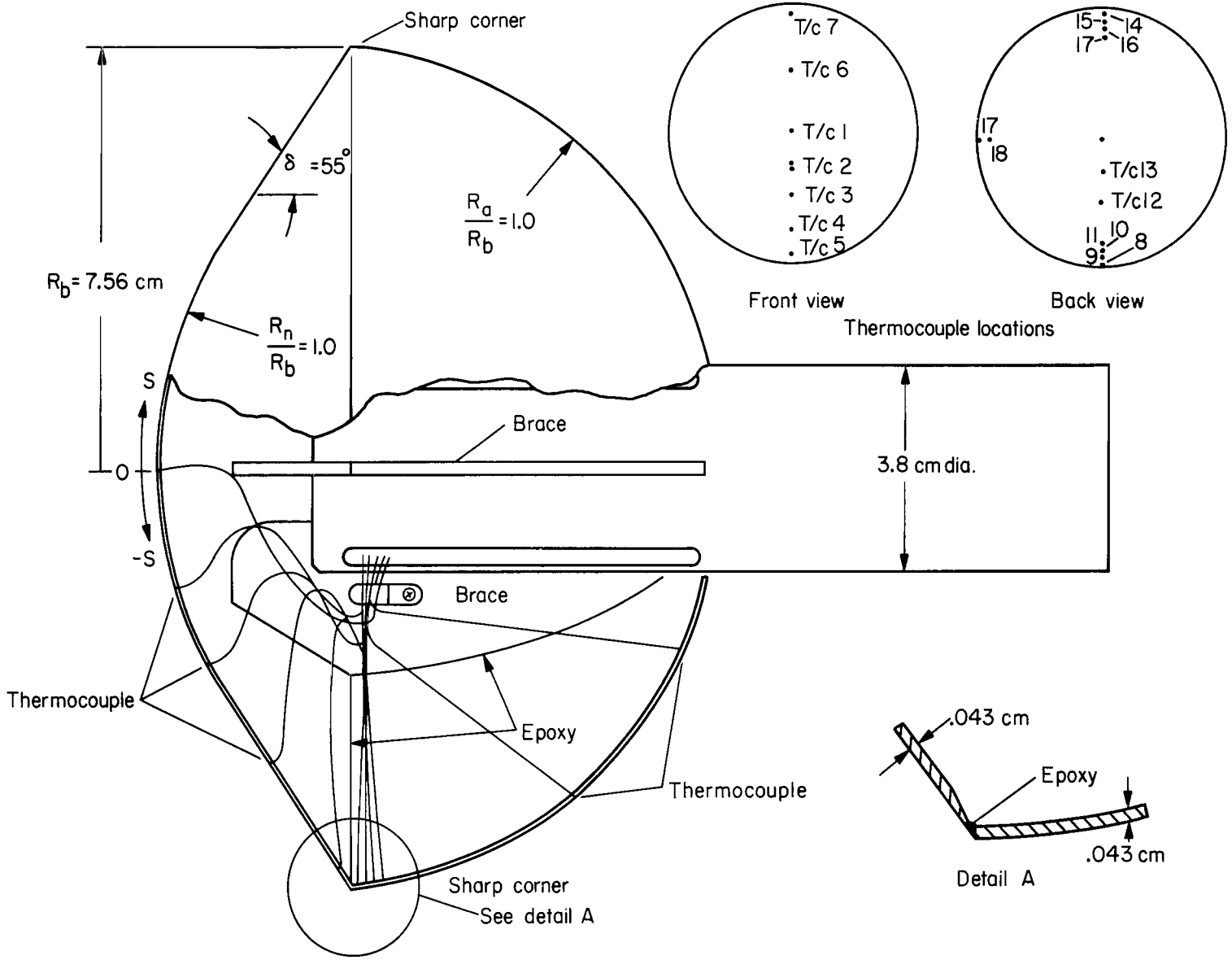


Figure 1.– Planetary atmosphere experimental test model.

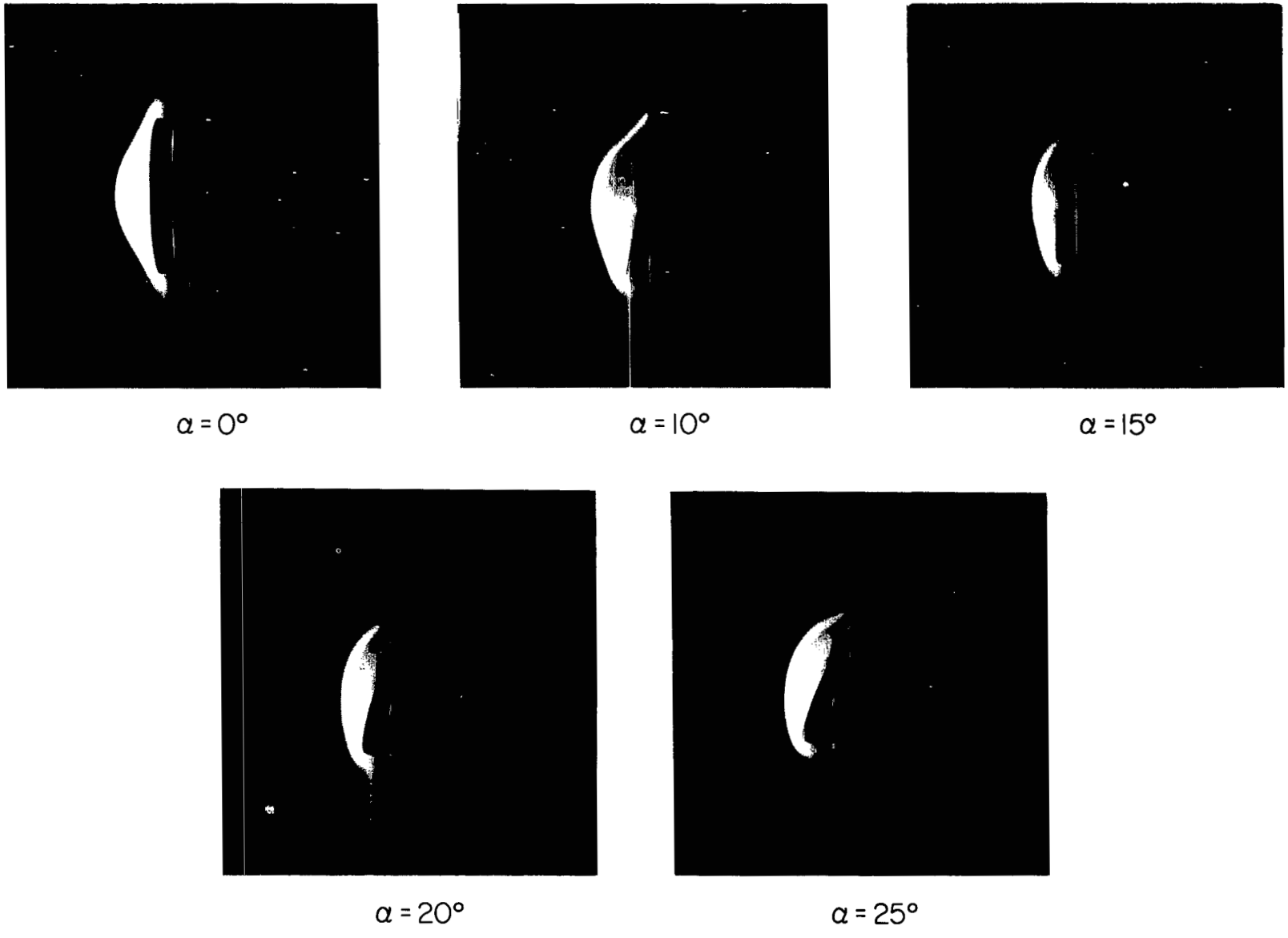


(a) PAET configuration; 42-inch shock tunnel at $M_\infty = 15$ and $Re_D = 15{,}500$.

Figure 2.– Flow visualization pictures and shadowgraphs of bow wave.

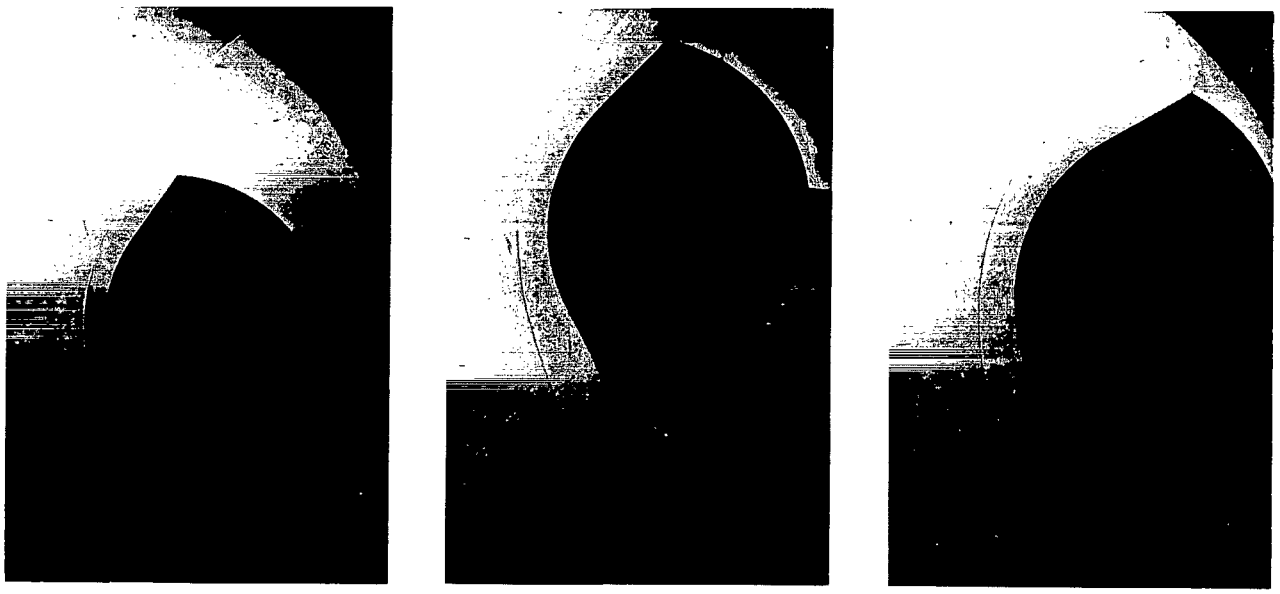

α = 0° α = 10° α = 25°

(b) PAET configuration; hypersonic free-flight facility at $M_\infty = 7$ and $Re_D = 100{,}000$.

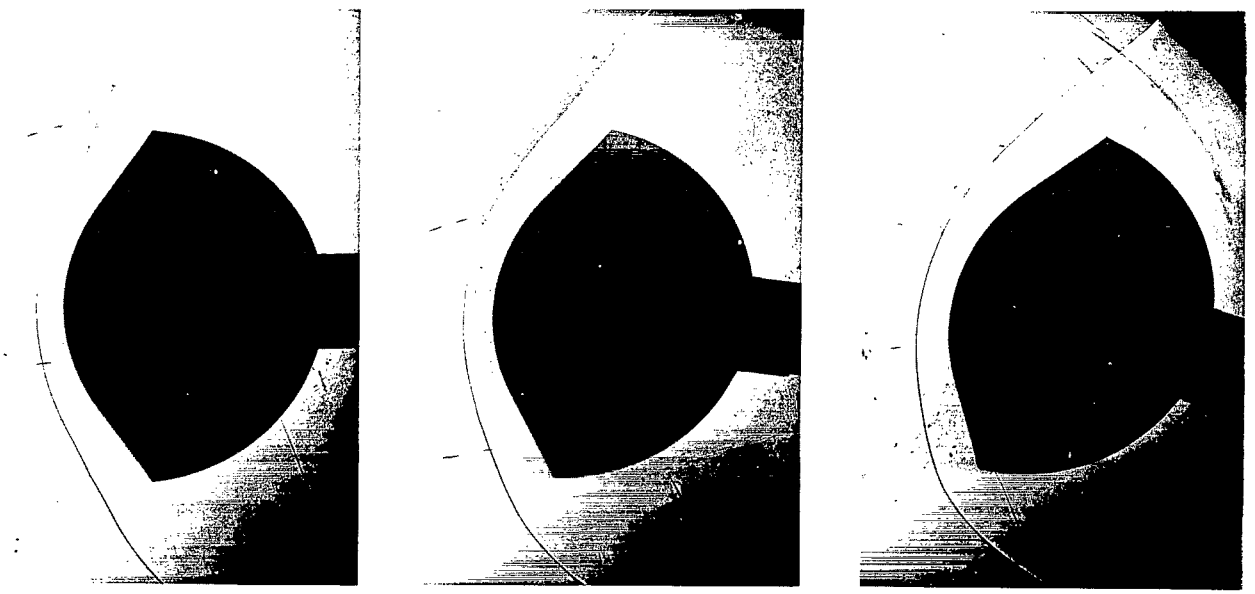

α = 0° α = 10° α = 20°

(c) PAET configuration; hypersonic free-flight facility at $M_\infty = 7$ and $Re_D = 300{,}000$.

Figure 2.– Concluded.

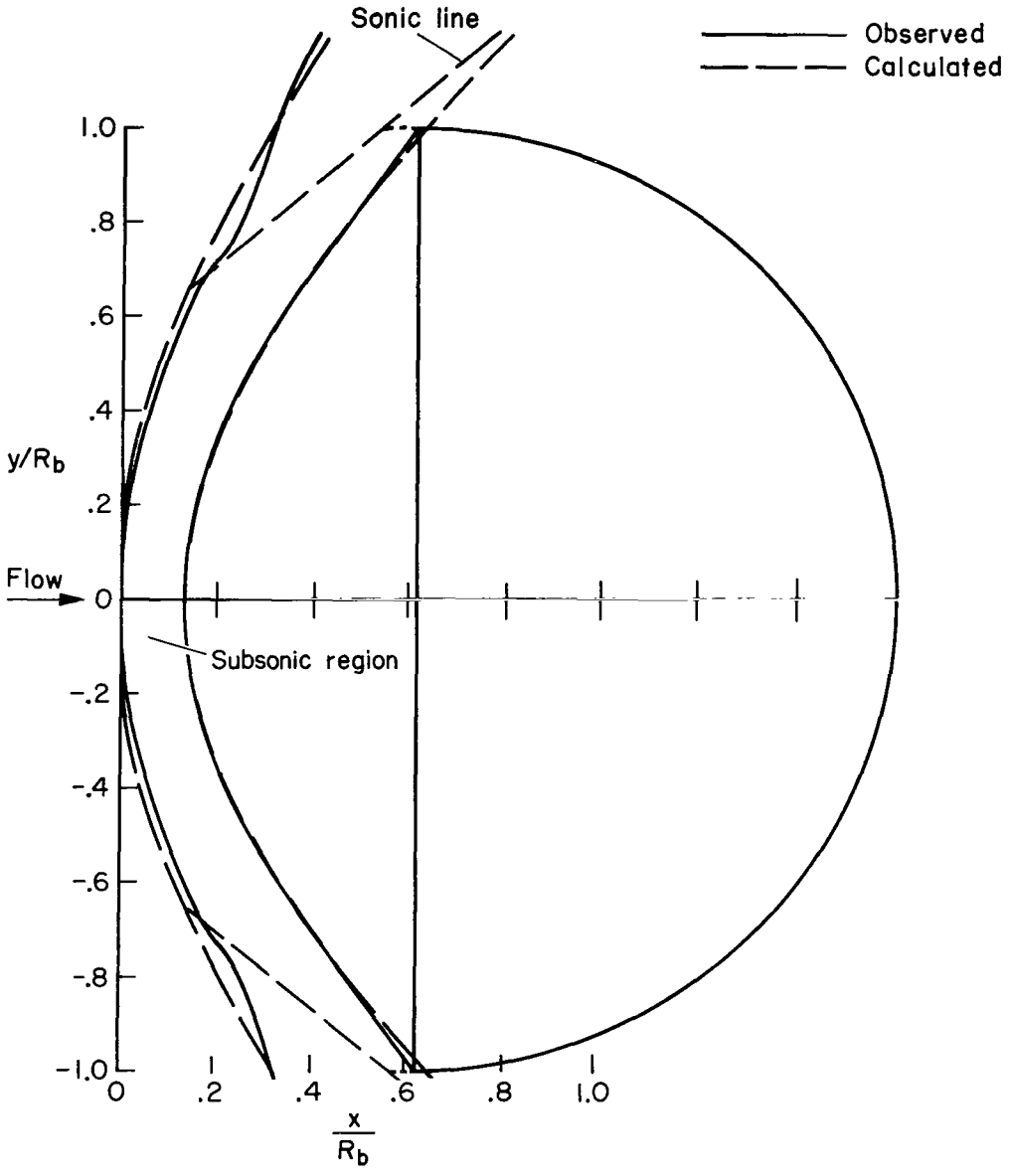


Figure 3.– Comparison of shock layer geometry with numerical prediction; $M_\infty = 7$, $Re_D = 1 \times 10^5$, $\alpha = 0°$.

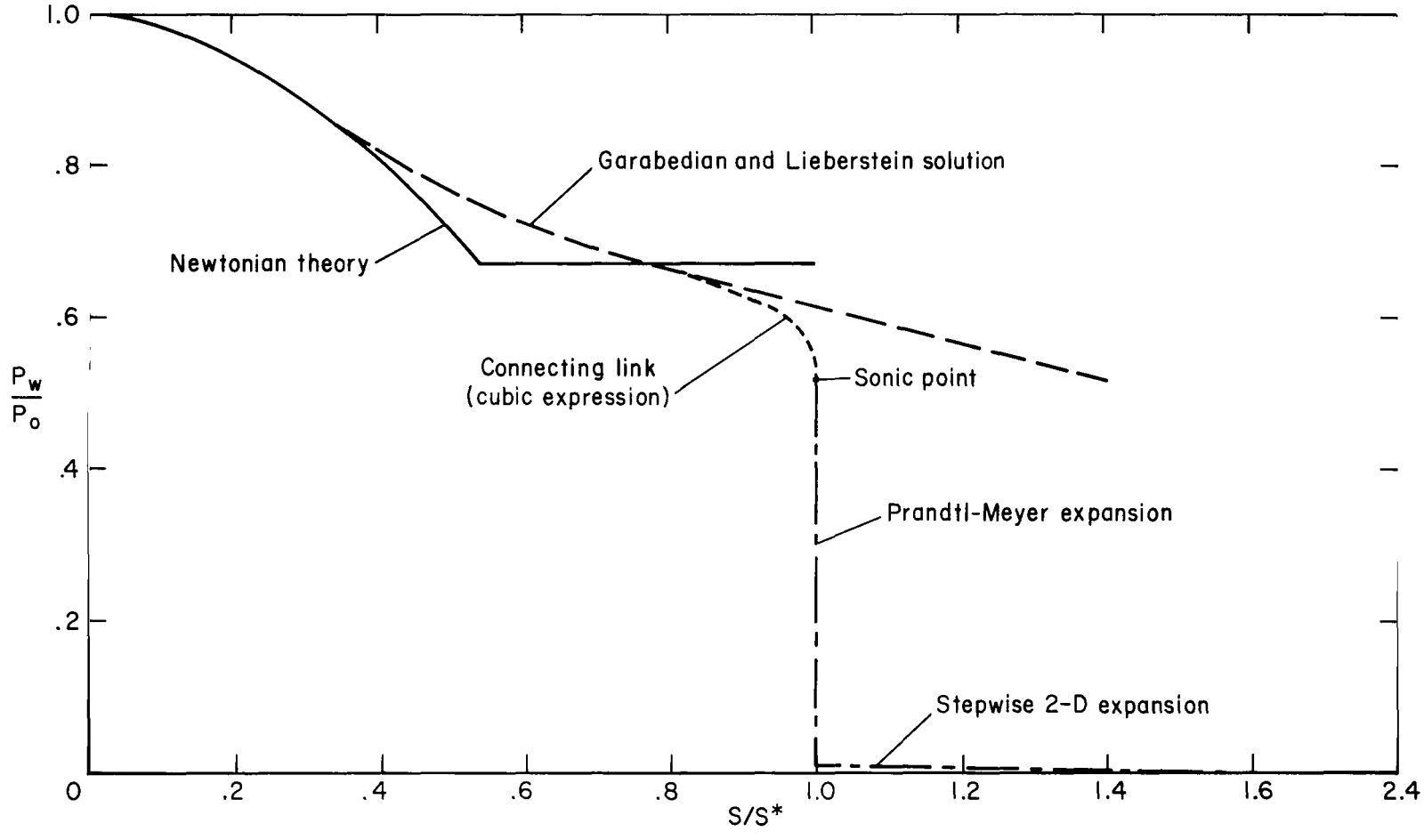


Figure 4.– Theoretical surface pressure distributions at $\alpha = 0°$.

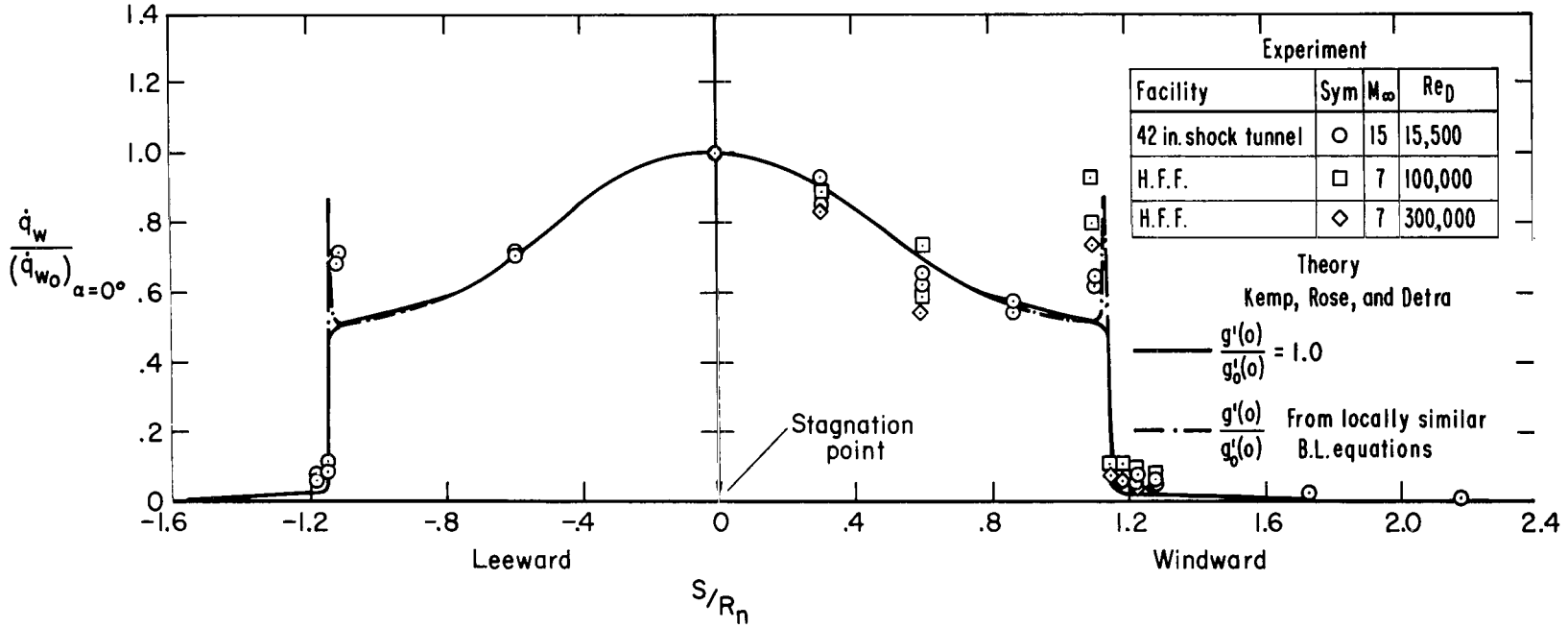


Figure 5.– Convective heat-transfer distribution over PAET body at $\alpha = 0°$.

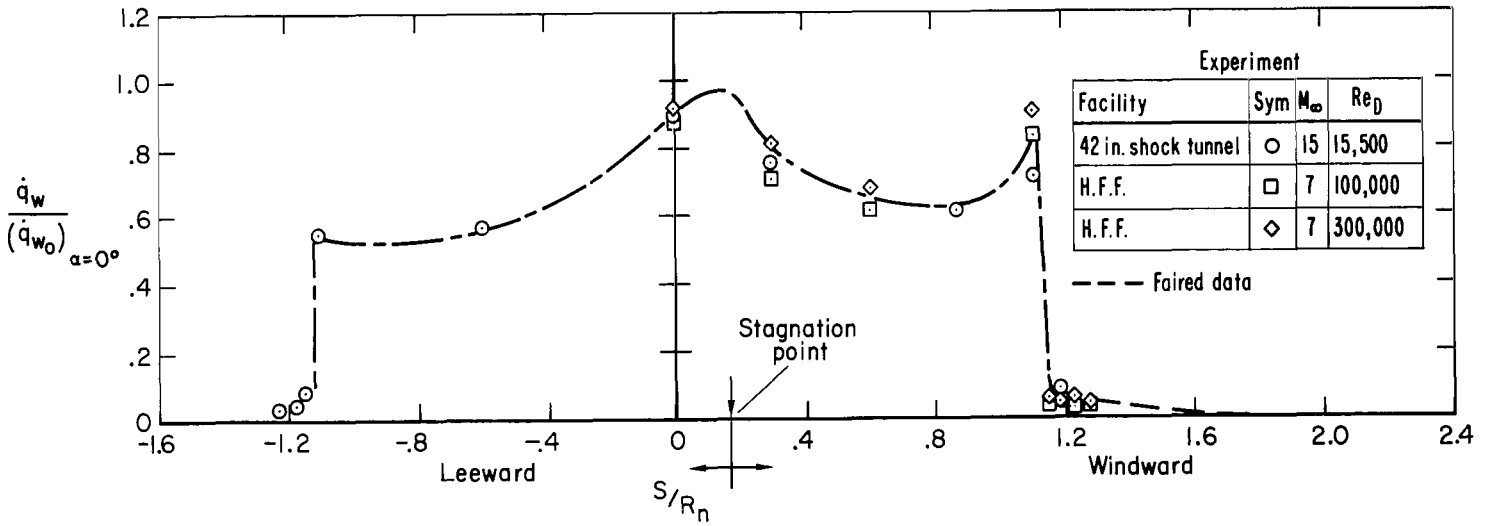


(a) $\alpha = 10°$

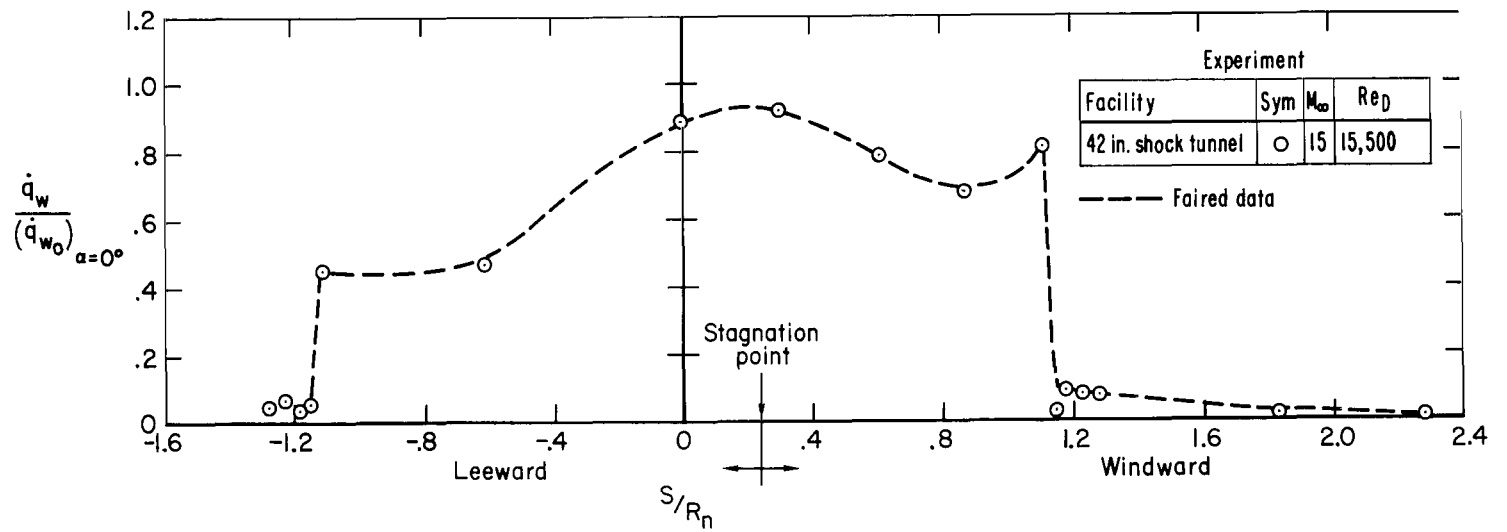


(b) $\alpha = 15°$

Figure 6.– Convective heating rates on PAET model at angle of attack from 10° to 25°.

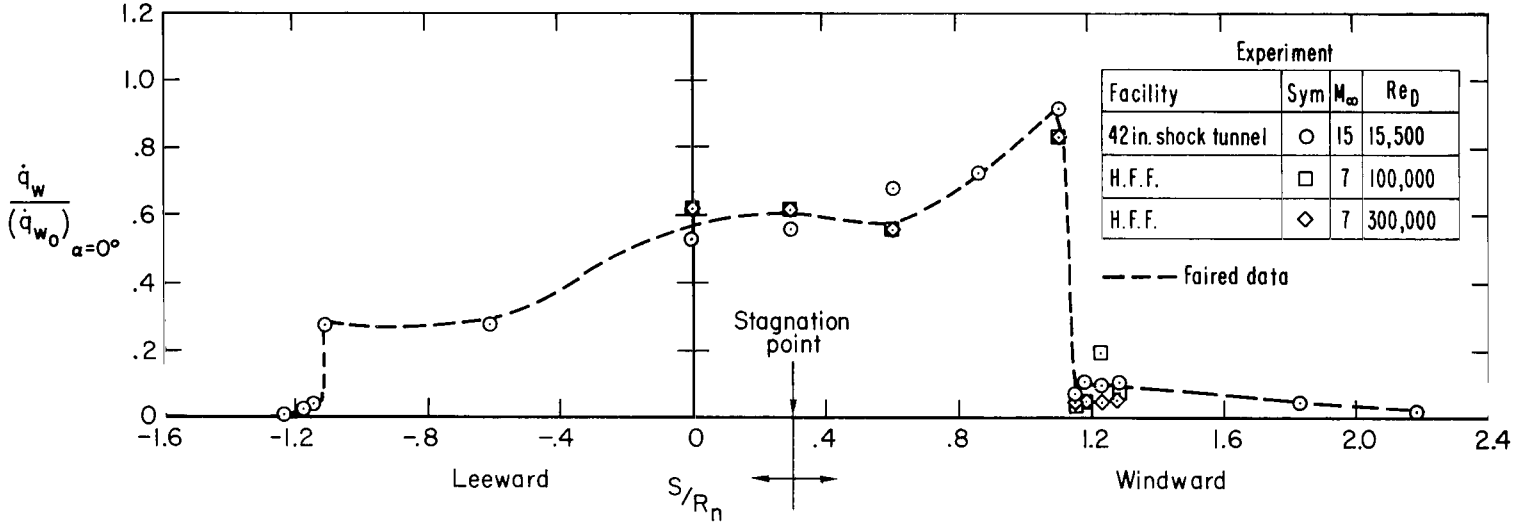


(c) $\alpha = 20°$

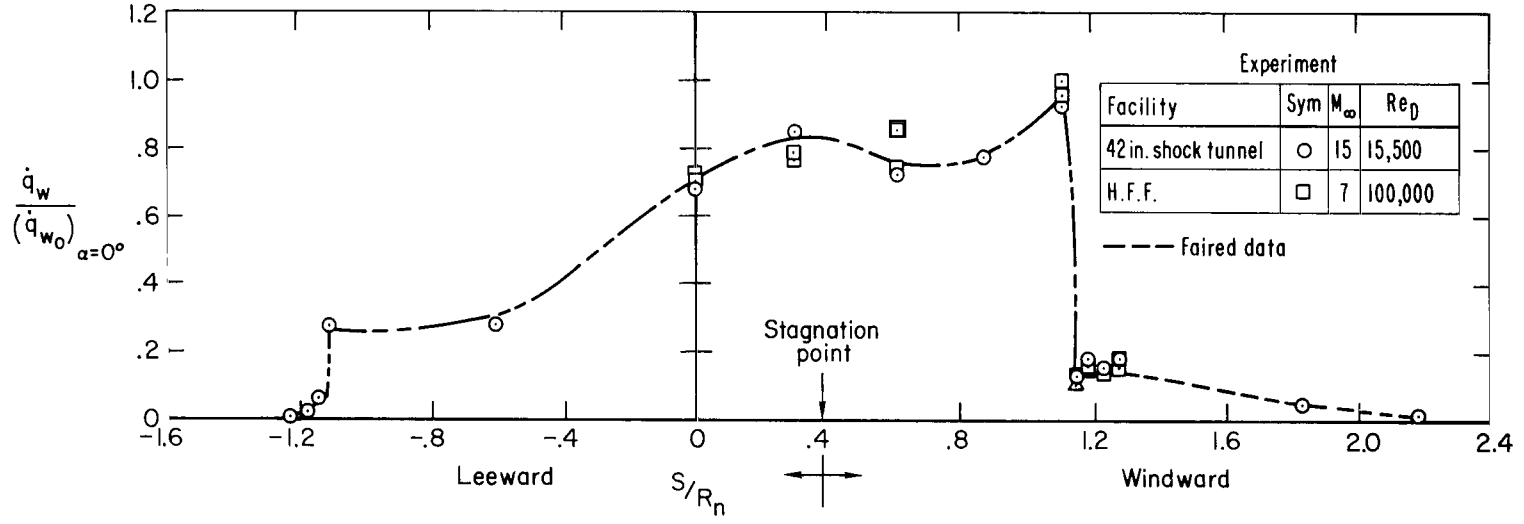


(d) $\alpha = 25°$

Figure 6.– Concluded.

07U 001 58 51 3DS 71166 00903
AIR FORCE WEAPONS LABORATORY /WLOL/
KIRTLAND AFB, NEW MEXICO 87117

ATT E. LOU BOWMAN, CHIEF,TECH. LIBRARY



*"The aeronautical and space activities of the United States shall be conducted so as to contribute . . . to the expansion of human knowledge of phenomena in the atmosphere and space. The Administration shall provide for the widest practicable and appropriate dissemination of information concerning its activities and the results thereof."*

—NATIONAL AERONAUTICS AND SPACE ACT OF 1958

# NASA SCIENTIFIC AND TECHNICAL PUBLICATIONS

TECHNICAL REPORTS: Scientific and technical information considered important, complete, and a lasting contribution to existing knowledge.

TECHNICAL NOTES: Information less broad in scope but nevertheless of importance as a contribution to existing knowledge.

TECHNICAL MEMORANDUMS: Information receiving limited distribution because of preliminary data, security classification, or other reasons.

CONTRACTOR REPORTS: Scientific and technical information generated under a NASA contract or grant and considered an important contribution to existing knowledge.

TECHNICAL TRANSLATIONS: Information published in a foreign language considered to merit NASA distribution in English.

SPECIAL PUBLICATIONS: Information derived from or of value to NASA activities. Publications include conference proceedings, monographs, data compilations, handbooks, sourcebooks, and special bibliographies.

TECHNOLOGY UTILIZATION PUBLICATIONS: Information on technology used by NASA that may be of particular interest in commercial and other non-aerospace applications. Publications include Tech Briefs, Technology Utilization Reports and Technology Surveys.

*Details on the availability of these publications may be obtained from:*

**SCIENTIFIC AND TECHNICAL INFORMATION OFFICE**

**NATIONAL AERONAUTICS AND SPACE ADMINISTRATION**

**Washington, D.C. 20546**